



UNIUNEA EUROPEANĂ



GUVERNUL ROMÂNIEI  
MINISTERUL MUNCII, FAMILIEI ŞI  
PROTECŢIEI SOCIALE  
AMPOSDRU



Fondul Social European  
POSDRU 2007-2013



Instrumente Structurale  
2007-2013



MINISTERUL  
EDUCAŢIEI  
CERCETĂRII  
ŞI SPORTULUI

OIPOSDRU



UNIVERSITATEA BABEŞ-BOLYAI  
CLUJ-NAPOCA

**Babeş-Bolyai University**  
**Faculty of Chemistry and Chemical Engineering**

**Synthesis, characterization and molecular modeling of some  
biopolymers**

**-PhD thesis-**

**PhD Candidate**  
**Izabella Irsai**

**Scientific advisor**

**Prof. Dr. Ioan Silaghi-Dumitrescu**

**Prof. Dr. Luminița Silaghi-Dumitrescu**

**Cluj-Napoca**  
**2012**



UNIUNEA EUROPEANĂ



GUVERNUL ROMÂNIEI  
MINISTERUL MUNCII, FAMILIEI ȘI  
PROTECȚIEI SOCIALE  
AMPOSDRU



Fondul Social European  
POSDRU 2007-2013



Instrumente Structurale  
2007-2013



MINISTERUL  
EDUCAȚIEI  
CERCETĂRII  
ȘI SPORTULUI

OIPOSDRU



UNIVERSITATEA BABEȘ-BOLYAI  
CLUJ-NAPOCA

# **Universitatea Babeș-Bolyai**

## **Facultatea de Chimie Și Inginerie Chimică**

### **Sinteza, caracterizarea și modelarea moleculară a unor biopolimeri**

**-teză de doctorat-**

**Doctorand  
Izabella Irsai**

**Conducători de doctorat**

**Prof. Dr. Ioan Silaghi-Dumitrescu**

**Prof. Dr. Luminița Silaghi-Dumitrescu**

**Cluj-Napoca  
2012**

# Contents

General Introduction.....	1
Chapter I Experimental studies on polylactic acid .....	2
I.2 Enzymatic synthesis of polylactic acid.....	3
1.2.1 Results and discussions .....	3
1.2.3 Conclusions.....	6
Chapter II Computational studies on polylactic acid.....	7
II.2. Studies on decameric units of PLA: in search of possible secondary structure-like motifs.....	8
II.2.2. Results and discussion.....	8
II.2.3. Conclusions.....	12
II. 3. A Ramachandran-like analysis of the geometry-optimized PLA decamers; comparison with the PLA-unique structure proposed by DeSantis .....	14
II.4. Inter-strand supramolecular interactions between PLA units.....	16
II.4.2. Results and discussion.....	16
II.4.3. Conclusions.....	23
II.5. Spectroscopic predictions on PLA secondary structure elements .....	25
II.5.3. Results and Discussion .....	25
II.5.4. Conclusions.....	29
II.6. Polylactic acid interactions with bioceramics surfaces .....	29
II.6.3. Results and discussions .....	30
II.6.4. Conclusions.....	35
Chapter III Study of polyethers by mass spectrometry.....	36
III.2 In-source collision induced dissociation study of polyethers cationized by alkali metal ions .....	37
III. 2.1 Experimental section .....	37
III.2.2 Results and Discussion .....	37
III.2.3 Conclusions.....	42
General conclusions .....	43
Acknowledgements.....	45
List of publications .....	46

## General Introduction

The goals of this study were the synthesis, characterization and molecular modeling of polylactic acid, polyethylene glycol and polypropylene glycol biopolymers.

This thesis consists of three chapters. The first two chapters are based on polylactic acid studies. The first chapter begins with an introduction about biopolymers and continues with experimental section which describes the enzymatic synthesis of polylactic acid.

The second chapter of the thesis contains computational studies on polylactic acid. It is composed of five main topics. The first three topics present computational results on the decameric units of polylactic acid: search of possible secondary structure-like motifs; a Ramachadran-like analysis of the geometry-optimized polylactic acid decamers, comparison with the PLA-unique structure proposed by DeSantis; inter-strand supramolecular interactions between polylactic units. The fourth topic summarizes literature data available for the vibrational analysis of polylactic acid and continues with spectroscopic predictions on polylactic acid secondary structure elements. The last topic presents results on the study of polylactic acid interactions with bioceramics surfaces.

The third chapter reviews the mass spectrometry studies of polyethylene glycol and polypropylene glycol described in the literature and presents the in-source collision induced dissociation study of polyethers cationized by alkali metal ions.

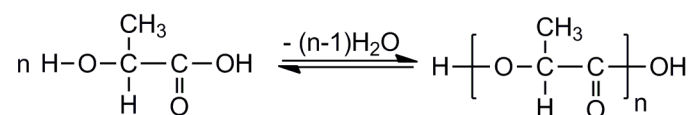
The thesis ends with the general conclusions and acknowledgements.

keywords: : polylactic acid, Candida Antarctica lipase B, molecular modeling, semiempirical, DFT, vibrational analysis, molecular dynamics, polyethylene glycol, polypropylene glycol, in-source collision induced dissociation

**Chapter I**  
**Experimental studies on polylactic acid**

## I.2 Enzymatic synthesis of polylactic acid

Enzymatic polymerization reactions of lactic acid were investigated (Scheme I.1). The reactions were performed in the presence of *Candida Antarctica* lipase B (Novozym 435) enzyme. For optimization of the reaction conditions, the following parameters were investigated: solvent effect, substrate concentration, reaction temperature, reaction time. The structure of products was investigated by IR, NMR and MALDI-TOF methods.



**Scheme I.1. Enzymatic polymerization reaction of polylactic acid**

### 1.2.1 Results and discussions

#### 1.2.1.1 Synthesis

30 mg Novozyme 435 enzyme was added to 1 ml solution containing 500 mM, 1000 mM and 1500 mM L or DL lactic acid and different solvents. The reaction was conducted in 1.5 ml microtubes at 40 °C temperatures under shaking (300 rpm). The used solvents were hexane and chloroform. After the removal of the enzyme the solvent was evaporated and washed with toluene.

#### *Temperature effect*

Temperature is another factor that influences the enzyme stability. A study was carried out to determine the optimal temperature on the activity of the enzyme. Therefore the synthesis was conducted at 30°C, 40 ° and 50 °C temperature. (Figure I.1)

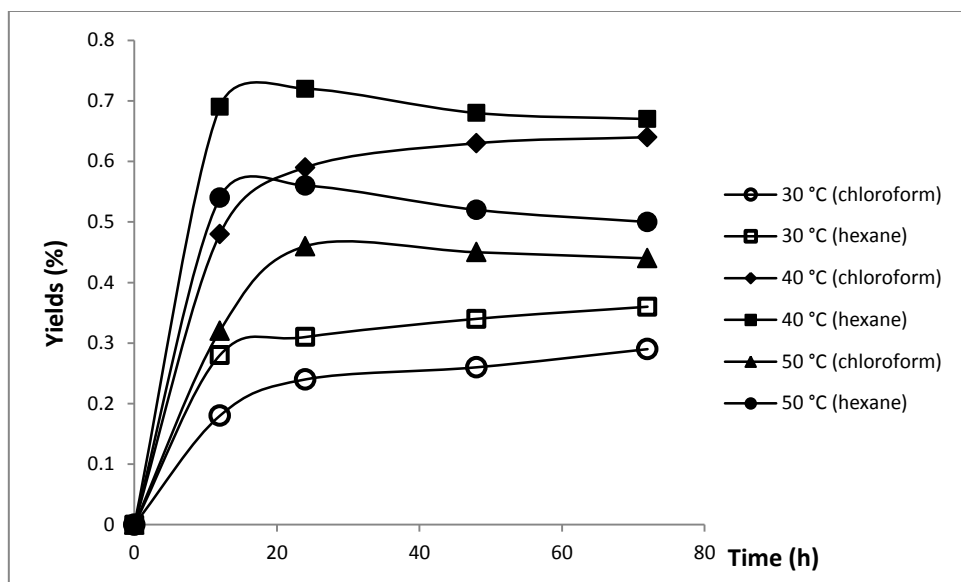
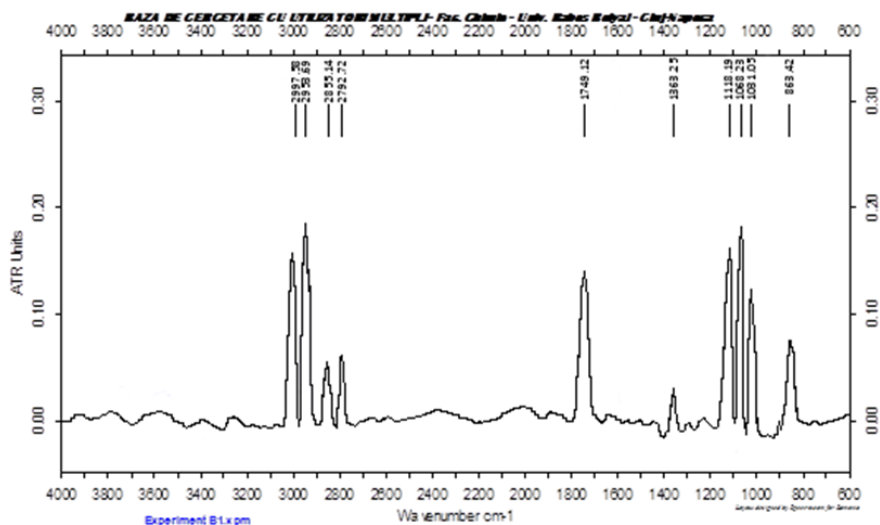


Figure I.1. The effect of temperature on the PLA synthesis

### 1.2.1.2. Structural analysis

#### IR studies

Figure I.2. IR spectra of poly(L-lactic acid) is showing the IR spectra of poly(L-lactic acid). The strong IR bands at 2997.58, 2953.69 and 2855.14  $\text{cm}^{-1}$  are assigned to the CH stretching region. These bands are attributed to the asymmetric  $-\text{CH}_3$ ,  $-\text{CH}$  and symmetric  $-\text{CH}_3$  stretching modes. In the IR spectra the  $\text{C}=\text{O}$  stretching region at about 1748.12  $\text{cm}^{-1}$ . The band at 1363.29  $\text{cm}^{-1}$  appears due to the  $-\text{CH}_3$  bending. The  $\text{C}-\text{OC}$  stretching mode of the ester group appears at 1068.23  $\text{cm}^{-1}$ .



## Figure I.2. IR spectra of poly(L-lactic acid)

### *NMR studies*

The  $^1\text{H}$  NMR spectra of lactic acid has two signals assigned to CH and  $\text{CH}_3$  at 4.03 and 1.23 ppm. These two assignments appear on the polylactic acid spectra obtained in  $\text{DMSO-d}_6$  at 5.17 and 1.46 in the case of PDLLA respectively 4.93 and 1.45 for PLLA. (Figure I.3) CO,  $\text{CH}_3$  and CH resonances are found in  $^{13}\text{C}$  NMR spectra at 171,72 ppm, 65,88 ppm and 16,71 in the case of PLLA respectively 169,02 ppm, 68,75 ppm and 16,41 ppm in the case of PDLLA.

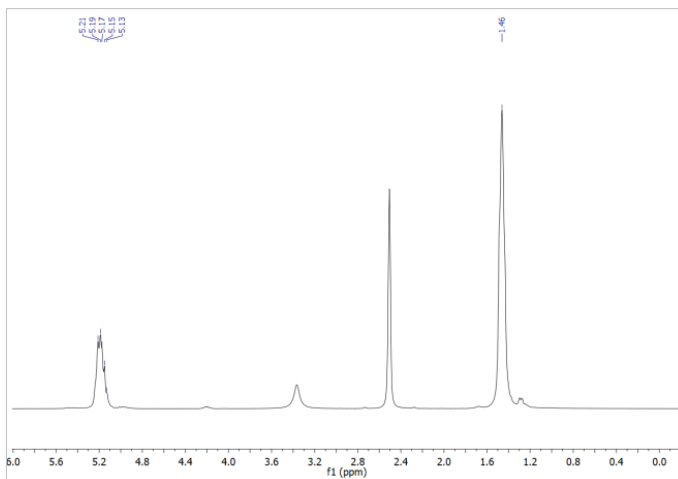


**Figure I.3.  $^1\text{H}$  NMR spectra of poly(DL-lactic acid)**

### *MALDI TOF analysis*

MALDI TOF MS has been employed for the determination of the molecular weights. With enzymatic reactions only low molecular weight oligomers can be prepared. Figure I.4 present a MALDI TOF mass spectra of the poly(DL-lactic acid) synthesized in hexane at 40 °C temperature for 72 hours. The spectra is dominated by a series of intense peaks ranging from a mass of 200 Da to a mass of 1100 Da corresponding to oligomers doped with  $\text{Na}^+$  ions of type  $\text{H}[\text{O}-\text{CH}(\text{CH}_3)-\text{CO}]_n-\text{OH}-\text{Na}$ . As can be seen on the spectrum the n values vary from 3 to 13. The n values represent the number of the monomers. On the spectra can be seen signals with 22 units greater than the sodiated adduct ions, that means that the examined polymer is carboxyl terminated.

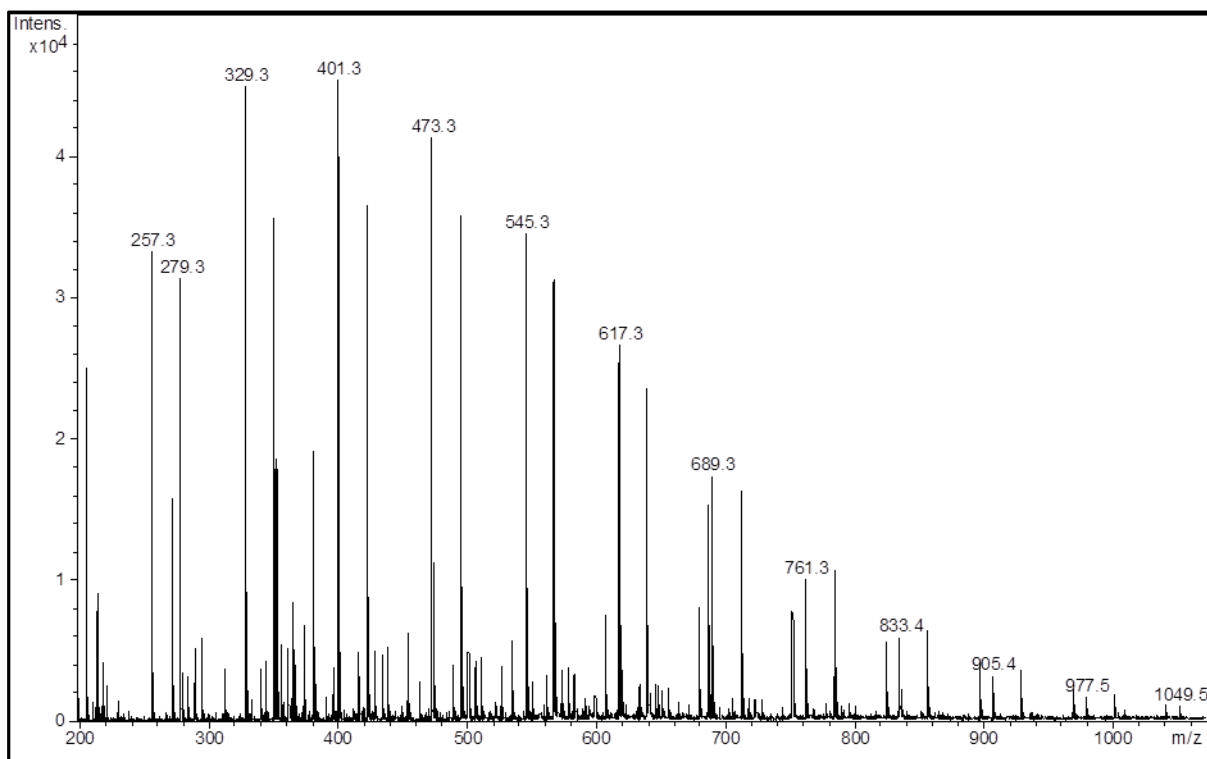


**Figure I.4. MALDI TOF spectra of PDLLA (temperature 40 °C, reaction time 72 h, solvent hexane)**

### 1.2.3 Conclusions

Immobilised lipase from *Candida antarctica* (Novozyme 435) was used to catalyze polymerization reactions of lactic acid. The influence of substrate concentration, solvent, temperature and reaction time were examined to determine the optimum conditions of synthesis. The best results were obtained by the polymerization of lactic acid at 40 °C, in the presence of hexane and at 24 h reaction time. The DL-lactic acid polymerization result oligomers with greater molecular weights than the poly(L-lactic acid).

**Chapter II**  
**Computational studies on polylactic acid**

## II.2. Studies on decameric units of PLA: in search of possible secondary structure-like motifs

The present study employs structures resulted from geometry optimization of four secondary-type structures helical structures ( $\alpha$ ,  $\pi$  and  $3_{10}$ ) as well as a  $\beta$ -sheet. These structures were built for the poly(L-lactic acid) (PLLA) as well as for the copolymer of poly(DL-lactic acid) (PDLA). Geometry optimizations were performed either in vacuum or with the CPCM continuum solvent model as implemented in Gaussian09 software package. The semiempirical PM6 method was employed as implemented in the Gaussian09 (labelled PM6-G in text) and MOPAC (labelled PM6-M in text) software packages.

### II.2.2. Results and discussion

Figure II.1 and Figure II.2 illustrate the optimized geometries.

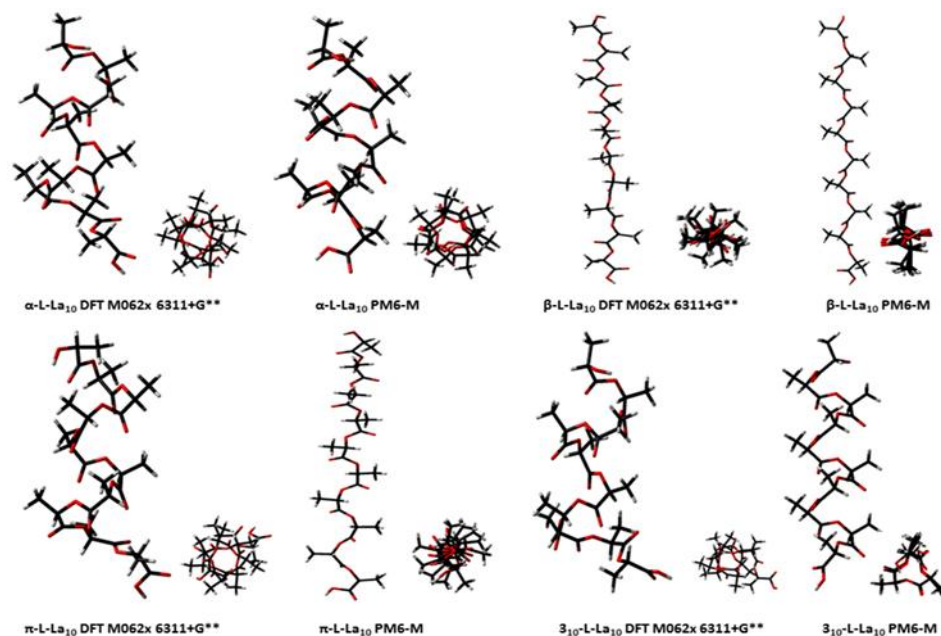
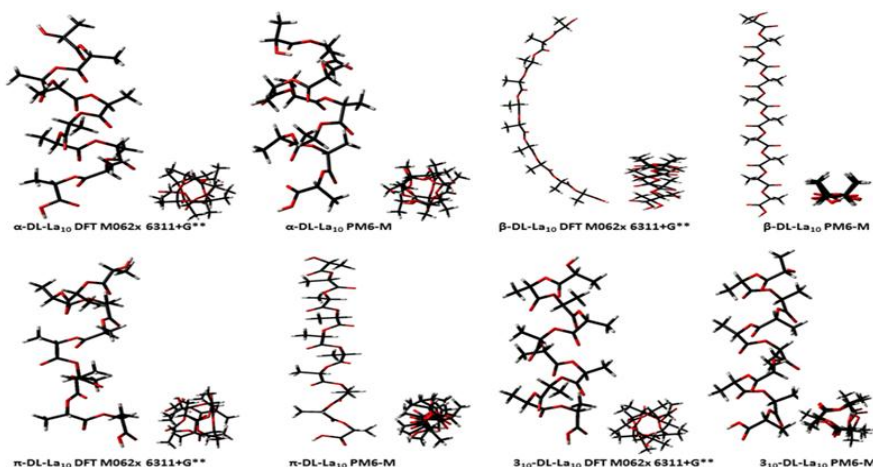


Figure II.1. Graphical representation of L-LA<sub>10</sub> geometries optimized by DFT and semiempirical methods



**Figure II.2. Graphical representation of DL-LA<sub>10</sub> geometries optimized by DFT and semiempirical methods**

### II.2.2.1. Energy

Comparing the calculated energy of PLLA with the energy of PDLLA it can be observed that the values in the case of PLLA are generally smaller (Table II.1), suggesting that such structures are more stable.

**Table II.1. The relative energies (kcal/mol) of PDLLA structures, and the relative energy obtained by subtracting the energy of the PDLLA decamer from that of the PLLA decamer.**

Methods	$\Delta E$				
	$\alpha$ -DL-LA <sub>10</sub>	$\pi$ -DL-LA <sub>10</sub>	10 <sub>3</sub> -DL-LA <sub>10</sub>	$\beta$ -DL-LA <sub>10</sub>	DL-L
MM UFF	0.4	16.2	0.0	2.5	19.9
PM6-G	-2.3	-5.4	0.0	-8.3	-4.6
PM6-M	-0.8	20.5	0.0	26.1	2.8
PM6-M solution	0.8	5.6	0.0	8.9	5.4
HF/3-21G*	0.2	3.2	0.0	13.2	18.7
HF/3-21G* water	0.1	0.4	0.0	3.5	13.8
HF/6-31G*	0.9	-0.3	0.0	1.5	28.8
DFT/B3LYP/6-31G*	22.0	23.1	n.a.	0.0	-4.7
DFT/M062x/6-31G*	0.9	-4.4	0.0	21.2	8.9
DFT/M062x/6-31G**	1.0	-4.6	0.0	21.6	8.5
DFT/M062x/6-31G** water	7.3	7.9	0.0	21.5	0
DFT/M062x/6-311+G**	1.6	4.4	0.0	19.6	41.3

### II.2.2.2. Chain length

The length of the decameric chain was measured between the ester oxygen atoms of the first monomer and the ester oxygen atoms of the ninth monomer (numbering starting from the OH terminus of the polylactide).

These lengths are shown in Table II.2 for PLLA. All the methods preserve the helix length of  $\alpha$ -L-LA<sub>10</sub> within  $\pm 1.5 \text{ \AA}$  of the initial structure.

**Table II.2. The helix lengths of PLLA**

Methods	Helix length( $\text{\AA}$ )					
	$\alpha$ -L-LA <sub>10</sub>		$\pi$ -L-LA <sub>10</sub>		10 <sub>3</sub> -L-LA <sub>10</sub>	
	initial	optimized	initial	optimized	initial	optimized
MM UFF	12.4	12.3	21.6	24.0	16.0	12.1
PM6-G	12.4	12.7	21.6	25.4	16.0	14.4
PM6-M	12.4	10.9	21.6	24.6	16.0	14.0
PM6-M solution	12.4	11.4	21.6	24.5	16.0	12.3
HF/3-21G*	12.4	12.6	21.6	16.7	16.0	12.7
HF/3-21G* water	12.4	13.8	21.6	16.2	16.0	n.a.
HF/6-31G*	12.4	13.9	21.6	14.2	16.0	14.3
DFT/B3LYP/6-31G*	12.4	13.3	21.6	14.0	16.0	13.9
DFT/M062x/6-31G*	12.4	12.0	21.6	12.1	16.0	12.1
DFT/M062x/6-31G**	12.4	12.0	21.6	12.1	16.0	12.0
DFT/M062x/6-31G** water	12.4	12.3	21.6	12.6	16.0	12.5
DFT/M062x/6- 311+G**	12.4	12.1	21.6	12.2	16.0	11.4

### II.2.2.3. Weak interactions

In terms of the non-covalent interactions dictating secondary structure preferences in poly(lactic acid), three kinds of intramolecular interactions can be expected in the models employed in the present study.

One of these weak interactions may involve the oxygen atom of the carbonyl group and the hydrogen atom from the main chain ( $\text{CO}\dots(\text{CH})_{n+1}$ ). These  $\text{CO}\dots(\text{CH})_{n+1}$  distances in the initial structures are between 2.75 and 2.90  $\text{\AA}$ , all of which exceed the 2.72  $\text{\AA}$  represented by the sum of the atomic van der Waals radii for the hydrogen and oxygen. However, after geometry

optimization these distances are less than 2.72 Å in all models; the average values are between 2.34 Å and 2.45 Å, implying attractive interactions even in the  $\beta$  structure (Tables II.5-8).

**Table II.3. CO...(CH)<sub>n+1</sub> lengths for  $\alpha$ -L-LA<sub>10</sub>. The initial value was 2.78 Å for all distances.**

O--H <sup>a</sup>	MM UFF	PM6-G	PM6-M	PM6-M water	HF 3-21G*	HF 3-21G* water	HF 6-31G*	DFT B3LYP 6-31G*	DFT M062x 6-31G*	DFT M062x 6-31G**	DFT M062x 6-31G** water	DFT M06/2x 6-311+G**
1-2	2.55	2.34	2.30	2.33	2.37	2.57	2.44	2.41	2.40	2.39	2.44	2.39
2-3	2.56	2.28	2.28	2.32	2.53	2.57	2.45	2.41	2.49	2.49	2.49	2.48
3-4	2.55	2.30	2.30	2.30	2.30	2.58	2.44	2.43	2.41	2.40	2.45	2.43
4-5	2.59	2.24	2.26	2.28	2.40	2.55	2.44	2.42	2.42	2.41	2.45	2.44
5-6	2.54	2.31	2.27	2.29	2.30	2.57	2.44	2.42	2.44	2.43	2.44	2.48
6-7	2.59	2.32	2.32	2.34	2.45	2.58	2.44	2.43	2.46	2.45	2.46	2.46
7-8	2.54	2.31	2.30	2.34	2.31	2.61	2.43	2.39	2.46	2.45	2.46	2.38
8-9	2.59	2.30	2.27	2.38	2.38	2.65	2.44	2.28	2.42	2.42	2.49	2.42
9-10	2.55	2.31	2.30	2.42	2.47	2.73	2.50	2.25	2.29	2.29	2.52	2.52

<sup>a</sup> lactic acids whose CO...(CH)<sub>n+1</sub> lengths are indicated in this column

One interesting parameter to follow, from the point of view of defining secondary structure elements, is the close contact CO..(-O)<sub>n+x</sub>, representing distances between oxygen atoms from carbonyl groups and oxygen atoms from the ester groups. The poly(lactic acid) polymer is similar to a polypeptide, except that the peptide bonds are now replaced by ester bonds. The polypeptide chain is stabilized by intramolecular hydrogen-bonds involving precisely the peptidic atoms, N(H) and O. The equivalents of these N---O distances are listed in Tables II.13-16; despite the repulsive interaction that one may have expected for a CO---O situation, these distances are, even with some of the more accurate DFT methods, at the limit of the sum of van der Waals radii (3.04 Å).

**Table II.4. CO..(-O)<sub>n+3</sub> length for 3<sub>10</sub>-L-LA<sub>10</sub>**

CO..(-O) <sub>n+3</sub>	Initial	MM UFF	PM6-G	PM6-M water	PM6-M	HF 3-21G*	HF 3-21G* water	HF 6-31G*	DFT B3LYP 6-31G*	DFT M062x 6-31G*	DFT M062x 6-31G**	DFT M062x 6-31G** water	DFT M06/2x 6-311+G**
1-4	2.83	3.22	3.51	3.44	3.39	3.11	n.a.	3.45	3.36	3.08	3.09	3.02	3.25
2-5	2.83	3.52	3.43	3.27	3.36	3.19	n.a.	3.47	3.35	3.11	3.10	3.10	3.24

3-6	2.82	3.25	3.49	3.44	3.41	3.66	n.a.	3.50	3.38	3.14	3.14	3.10	3.06
4-7	2.83	3.56	3.47	3.31	3.38	3.34	n.a.	3.52	3.44	3.17	3.17	3.09	3.26
5-8	2.83	3.18	3.47	3.44	3.39	3.26	n.a.	3.47	3.32	3.20	3.21	3.14	3.10
6-9	2.83	3.71	3.49	3.39	3.42	3.17	n.a.	3.32	3.22	3.04	3.04	3.14	3.07
7-10	2.83	3.29	3.48	3.65	3.46	3.47	n.a.	3.56	3.58	3.10	3.11	3.06	4.43

The third type of non-covalent interaction involves the oxygen atoms from carbonyl groups and the hydrogen atoms from the methyl groups.

In the initial structure of  $\pi$ -L-LA<sub>10</sub> the CO...(CH<sub>3</sub>) distances are around 7 Å (Table II.5). The MM and PM6 methods tend to conserve these non-bonding distances, while HF and DFT distinctly shorten them, to less than the corresponding sum of van der Waals radii.

**Table II.5. CO...(CH<sub>3</sub>)<sub>n+3</sub> length for  $\pi$ -L-LA<sub>10</sub>. The initial value was 7.11 Å for all distances.**

CO...(CH <sub>3</sub> ) <sub>n+3</sub>	MM UFF	PM6-G	PM6-M water	PM6-M	HF 3-21G*	HF 3-21G* water	HF 6-31G*	DFT B3LYP 6-31G*	DFT M062x 6-31G*	DFT M062x 6-31G**	DFT M062x 6-31G** water	DFT M06/2x 6-311+G**
1-4	8.03	9.17	8.07	8.10	2.45	2.48	3.06	3.34	2.65	2.66	2.42	2.54
2-5	7.86	9.28	8.01	8.06	5.01	4.91	2.76	2.62	2.40	2.40	2.43	2.42
3-6	7.99	9.27	8.00	7.96	2.45	3.77	2.84	2.75	2.43	2.42	2.44	2.46
4-7	8.03	9.27	7.94	7.91	5.11	2.49	2.80	2.59	2.41	2.41	2.42	2.41
5-8	7.87	9.27	7.97	7.93	2.44	4.88	2.78	2.58	2.52	2.51	2.51	2.57
6-9	7.86	9.33	8.13	8.29	5.10	3.72	2.80	2.64	3.12	3.11	3.10	2.57
7-10	8.49	9.13	8.04	8.47	2.43	2.47	2.69	2.58	2.54	2.52	2.35	3.54

## II.2.3. Conclusions

The data shown here illustrates that protein-like secondary structure elements may be feasible in short decameric stretches of polylactic acid. Importantly, computational predictions on the relative stabilities and structural details differ significantly between empirical, semiempirical and ab initio methods. Even between two DFT methods, B3LYP and M062x, significant qualitative differences were noted for some of the structures. These observations underline significant difficulties in accurate predictions on structures whose integrity relies exclusively on

weak, non-covalent interactions. Solvation, using water as solvent, appears to lead to a slight, but detectable elongation of the weak contacts.

The highest-level methods employed here predict that  $\alpha$ ,  $\pi$  and  $10_3$  structures have very similar energies, with  $\pi$  slightly favored by values within the error limits of the method; this is in contrast with results obtained with less accurate semiempirical and empirical methods, which predict larger differences and other structures as favorites. Relative energies of poly-L and poly-D,L lactic acid structures indicate the former to be energetically-favored over the latter.

The details of structural features predicted by empirical, semiempirical and ab initio methods also differ in some of the cases. Three types of weak interactions appear to dictate the relative stabilities of secondary structure elements in polylactic acid structures. These non-covalent interactions involve the oxygen atom of the carbonyl group and atoms of neighboring monomers in the primary structure, as follows: (1) the hydrogen atom of the CH group in lactic acid, (2) a hydrogen atom in the methyl group, and (3) the oxygen atom of an ester group.

## II. 3. A Ramachandran-like analysis of the geometry-optimized PLA decamers; comparison with the PLA-unique structure proposed by DeSantis

The helical conformation of the polylactic acid was analyzed by DeSantis and coworkers. They investigated the X ray structure of poly(S lactic acid). The conformation fits a helix characterized by ten monomeric units in three turns and a monomeric repeat on the helical axis equal to 2.78 Å. The structure proposed by DeSantis was optimized in addition to the four decameric units.

The empirical and semiempirical PM6 methods predict the structure DeSantis to be the less stable one. The HF methods anticipate the  $\beta$ -L-LA<sub>10</sub> sheet the most stable, it is followed by the DeSantis structure. The density functional methods change the preference: they support that the DeSantis structure as the most stable. Enlarging from a double-zeta basis set to a triple-zeta basis set with diffuse functions increase the energy differences between the DeSantis structure and the other four structures, especially in the case of PDLA.

The initial chain length is 18.92 Å. All methods elongate the helix with 3.48 – 3.78 Å. The MM and PM6 methods generate DeSantis helix length close to  $\pi$ -L-LA<sub>10</sub>. The HF methods give helix lengths longer with 6.2-10.5 Å than the length of  $\alpha$ ,  $\pi$  and 3<sub>10</sub> helices. The helix length calculated with DFT methods are also longer with 10-16 Å.

In addition to  $\alpha$  helix and  $\beta$  sheet secondary structures, another distinct structural motif has been distinguished in which the polypeptide chain reverses direction over the span of only a few amino acids. Such structures are known as ‘turns’. The turns are formed in the proteins due to the hydrogen bond between the main chain C=O and the N-H. In the optimized structures of  $\alpha$ ,  $\pi$  and 3<sub>10</sub> helices occur non-covalent interactions that involve the oxygen atoms from carbonyl groups (i) and the hydrogen atoms from the methyl groups (i+3). This fact leads to the conclusion that  $\beta$  turn could be formed in these three helices.

The two methods used in the optimization of  $\alpha$  helix give two types of results (Table II.6). The  $\Phi$  and  $\Psi$  values of the HF optimized  $\alpha$  helix indicates a type I  $\beta$  turn; the deviations from the

ideal values are bigger in the case of PLLA. The DFT/M062x method suggests a type III  $\beta$  turn. The  $\Phi$  and  $\Psi$  values are much closer to the ideal values than in the HF optimized structures.

**Table II.6.  $\Phi$  and  $\Psi$  angle values of the HF and DFT optimized  $\alpha$ -helix (initial values are -58 and -47)**

HF 3-21G*							
PLLA				PDLLA			
$\Phi_{i+1}$	$\Psi_{i+1}$	$\Phi_{i+2}$	$\Psi_{i+2}$	$\Phi_{i+1}$	$\Psi_{i+1}$	$\Phi_{i+2}$	$\Psi_{i+2}$
-95	6	-68	-10	-62	-25	-79	-3
-119	16	-76	3	-62	-33	-100	15
-119	9	-71	-9	-58	-27	-99	6
-105	9	-80	17	-55	-31	-102	19
DFT/M062x/6-31G**							
PLLA				PDLLA			
$\Phi_{i+1}$	$\Psi_{i+1}$	$\Phi_{i+2}$	$\Psi_{i+2}$	$\Phi_{i+1}$	$\Psi_{i+1}$	$\Phi_{i+2}$	$\Psi_{i+2}$
-71	-24	-68	-31	-58	-35	-70	-25
-74	-24	-75	-27	-55	-42	-73	-19
-73	-29	-71	-29	-58	-38	-79	-16
-73	-27	-73	-20	-57	-34	-104	-24

$\delta$  turns may exist in optimized  $\beta$  sheets (Table II.7). The  $\Phi$  and  $\Psi$  angles of the optimized  $\beta$  sheets have very close values to each other in both polylactic acids. The  $\Phi$  and  $\Psi$  values are -180 and -70° when the  $\beta$  sheet is optimized with HF method. These angles change their values to -153 and -178 in the DFT optimized structures.

**Table II.7.  $\Phi$  and  $\Psi$  angle values of the HF and DFT optimized  $\beta$  sheet (initial values are 180 and 180)**

HF 3-21G*							
PLLA				PDLLA			
$\Phi_{i+1}$	$\Psi_{i+1}$	$\Phi_{i+2}$	$\Psi_{i+2}$	$\Phi_{i+1}$	$\Psi_{i+1}$	$\Phi_{i+2}$	$\Psi_{i+2}$
-70	180	-71	-180	158	-179	-158	179
-71	-179	-71	-179	158	-180	-158	180
-71	-179	-71	-179	158	-180	-158	180
-71	-180	-71	-180	158	-179	-158	180
DFT/M062x/6-31G**							
PLLA				PDLLA			
$\Phi_{i+1}$	$\Psi_{i+1}$	$\Phi_{i+2}$	$\Psi_{i+2}$	$\Phi_{i+1}$	$\Psi_{i+1}$	$\Phi_{i+2}$	$\Psi_{i+2}$
-153	-178	-150	-177	156	177	-155	-175
-153	-178	-152	-178	157	-179	-154	-174
-152	-176	-149	-177	157	177	-157	-176
-153	-177	-147	-176	157	178	-156	-179

## II.4. Inter-strand supramolecular interactions between PLA units

This section attempts a molecular-level investigations of the inter-chain weak interactions involving PLA units, as part of an effort ultimately aiming to provide useful data for predicting and controlling macroscopic properties of PLA-based materials.

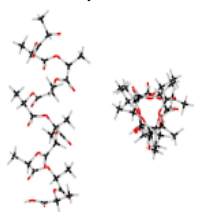
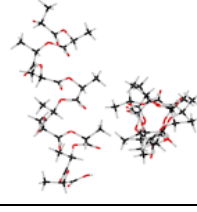
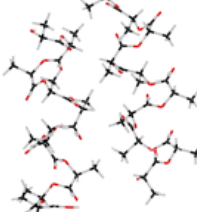
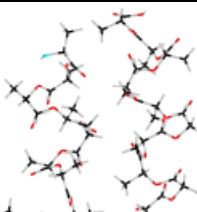
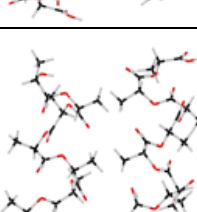
### II.4.2. Results and discussion

#### II.4.2.1. Perpendicular dimers

In the case of the perpendicular dimers a subsequent rotation by  $90^\circ$  was performed. Two types of input geometries were built; one is based on the canonical form and the other is based on the HF 3-21G\* optimized monomers.

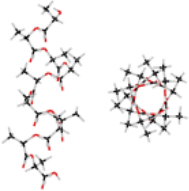
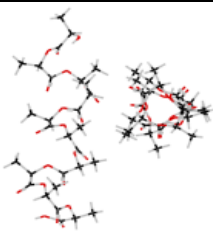
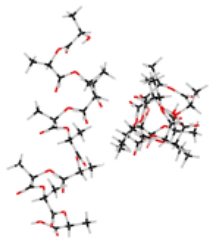
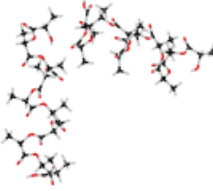
$\alpha$  dimers were constructed by translating the monomer unit by 2-6 Å. If the two monomers are situated at an initial 2-3 Å, the perpendicular direction is preserved and four weak interactions between the monomers are established in each of these cases. If the initial structure is based on the the optimized monomers, only C=O $\cdots$ H(CH<sub>3</sub>) interactions are established. However if the optimization is started from a structure in which the two optimized monomers are in perpendicular position at an initial 4-5 Å distances the two units will become almost parallel and the number of interactions between the two units increase at least seven (Table II.8). The difference between the two structures is in the type of the interactions. At the 4-Å laid monomers there is one more C=O $\cdots$ H interaction compared to the 5-Å laid monomers, while the latter has one O(carboxyl) $\cdots$ H interaction more. The more weak the interactions, the more stabilized are the structures, so that the parallel structures are more stable by around 8 kcal/mol as compared to those that remained perpendicular. Overall, each intermolecular interaction adds around 2 kcal/mol to the stabilization energy.

**Table II.8. Relative energies, weak interactions and the graphical representations of the perpendicular  $\alpha$ -dimers (initial structure based on HF/3-21 G\* optimized monomers), as resulted from unrestricted geometry optimizations. Initial distances (Å) between the monomers (before geometry optimizations) are shown.**

Initial structure based on HF/3-21G* optimized monomers						
						
Distance (Å)	$\Delta E$	C=O...H(CH)	C=O...H(CH <sub>3</sub> )	Other interactions	Length (Å)	Graphical representation
2	8.41		O42-H119		2.38	
			H44-O117		2.48	
			H73-O117		2.58	
			O69-H129		2.37	
3	8.47		O42-H119		2.36	
			H44-O117		2.44	
			H73-O117		2.59	
			O69-H129		2.36	
4	17.58	O5-H151			2.23	
		H13-O144			2.36	
			H18-O171		2.44	
			O33-H156		2.59	
		H40-O117			2.24	
			O42-H119		2.48	
5	16.56			H71-O94(hyd)	2.53	
		O5-H151			2.29	
				H7-O180(carb)	2.53	
			O33-H129		2.61	
		H40-O117			2.16	
			O42-H119		2.49	
			H45-O144		2.51	
6	14.69		O15-H146		2.35	
			O15-H175		2.55	
			H17-O144		2.47	
			H19-O171		2.61	
		O42-H115			2.29	
			H44-O117		2.41	
			O69-H120		2.34	
			H81-O108		2.59	

For the 6 Å dimers the two optimized structures are totally different, the structure based on canonical form is preserved perpendicular (Table II.9), but the monomers are shifted and connections are established between the endings. These don't form interactions between the carboxylic oxygen and hydrogen. The resulting structure from the optimization of the 2 Å distance positioned monomers is perpendicular, but if the two monomers are at 3 Å they are nearly perpendicular. The explanation lies in the increased numbers of interactions. Only C=O...H(CH) and C=O...H(CH<sub>3</sub>) interactions hold the molecules together. The interaction energies are around 1.5 kcal/mol.

**Table II.9. Relative energies, weak interactions and the graphical representations of the perpendicular  $\alpha$ -dimers (initial structure based on canonical form)**

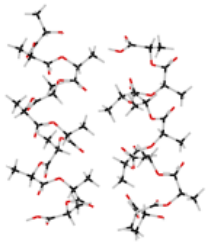
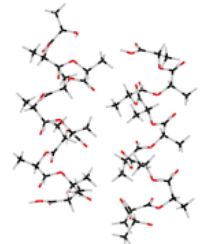
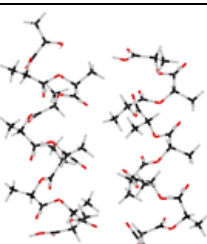
Initial structure based on canonical form					
					
Initial distance (Å)	$\Delta E$	C=O...H(CH)	C=O...H(CH <sub>3</sub> )	Length (Å)	Graphical representation
2	7.53	O24-H169		2.48	
			O24-H174	2.62	
			H26-O162	2.33	
		H31-O135		2.33	
			O33-H147	2.61	
3	9.58		O24-H169	2.45	
			O24-H174	2.52	
			H26-O162	2.41	
		H31-O135		2.20	
		O33-H142		2.44	
			O51-H173	2.65	
	H63-O144	2.45			
6	11.31		H28-O171	2.34	

#### II.4.2.2. Antiparallel dimers

A rotation by  $180^\circ$  was performed in the case of the antiparallel dimers. The geometry optimizations were carried out starting from structures based on canonical forms as well as on HF/3-21G\*-optimized monomers. In most cases, starting from the canonical form the convergence could not be achieved, and therefore only the results of the dimers of HF optimized monomers are discussed here.

Upon geometry optimization of the  $\alpha$  dimers, it can be observed that regardless of how far the dimers are placed (3-5 Å), one obtains the same results - they remain antiparallel and the relative energy, the weak interaction lengths have identical values. The two units are stabilized by six weak interactions; five of them are  $\text{C}=\text{O}\cdots\text{H}(\text{CH}_3)$  and one  $\text{C}=\text{O}\cdots\text{H}(\text{CH})$ . Each intermolecular interaction brings around 3 kcal/mol in terms of energy stabilization. (Table II.10)

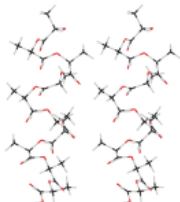
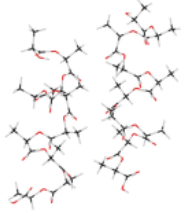
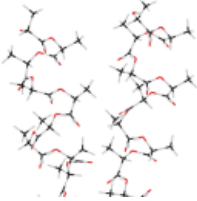
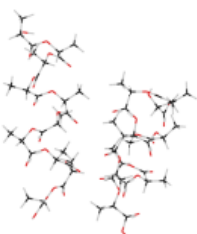
**Table II.10. Relative energies, weak interactions and the graphical representations of the antiparallel  $\alpha$ -dimer**

Initial structure based on HF/3-21G* optimized monomer					
Distance (Å)	$\Delta E$	C=O...H(CH)	C=O...H(CH <sub>3</sub> )	Length (Å)	Graphical representation
3	18.14		O24-H165	2.43	
			H26-O153	2.35	
		O51-H133		2.28	
		H53-O126	2.30		
		O78-H111	2.58		
		H80-O98	2.34		
4	18.14		O24-H165	2.43	
			H26-O153	2.35	
		O51-H133		2.28	
		H53-O126	2.30		
		O78-H111	2.58		
		H80-O98	2.34		
5	18.14		O24-H165	2.43	
			H26-O153	2.35	
		O51-H133		2.28	
		H53-O126	2.30		
		O78-H111	2.58		
		H80-O98	2.34		

### II.4.2.3. Parallel dimers

The parallel structures were obtained by translating a decameric unit with 1-6 Å. The optimized  $3_{10}$  monomers remain parallel if the two units are placed at 1-3 Å, but they are slightly shifted relative to one another (Table II.11). The dimer is held together by C=O...H(CH) and C=O...H(CH<sub>3</sub>) weak interactions. The intermolecular energy is around 2 kcal/mol in every case. On the other hand, upon increasing the distance to 4 Å the interactions are more numerous and now the shift of the two monomers is not so visible.

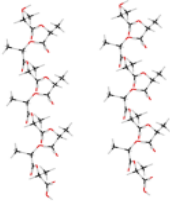
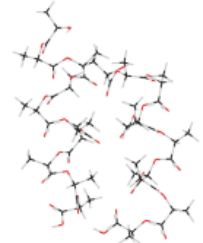
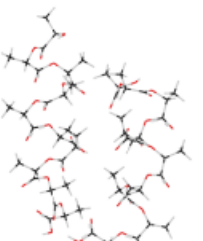
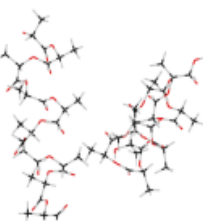
**Table II.11. Relative energies, weak interactions and the graphical representations of the parallel  $3_{10}$ -dimer (initial structure based on HF/3-21G\* optimized monomers)**

Initial structure based on HF/3-21G* optimized monomer					
					
Distance (Å)	$\Delta E$	C=O...H(CH)	C=O...H(CH <sub>3</sub> )	Length (Å)	Representation
1	11.77		O15-H146	2.69	
			H17-O117	2.41	
		O42-H151		2.28	
			H54-O144	2.39	
			O69-H182	2.51	
			H81-O171	2.51	
2	12.47	O42-H151		2.55	
			H44-O144	2.40	
			H45-O117	2.62	
			O69-H175	2.43	
			O69-H183	2.55	
3	11.95		H44-O117	2.37	
		O69-H151		2.16	
		H76-O144		2.33	
			O78-H183	2.45	
			H80-O171	2.62	
4	14.9		H17-O117	2.41	
		O42-H151		2.47	
			H46-O117	2.70	
		H49-O144		2.65	
			H54-O144	2.55	
		O69-H151		2.70	
		H76-O153		2.29	

The  $3_{10}$  monomers based on canonical form placed at 2-4 Å maintain the parallel orientation, but the two molecules are shifted with respect to each other. When the monomers are laid at 1-3 Å the first molecule's carbonyl groups are receded relative to the second molecules. The carboxyl group is also involved in inter-monomer interactions. The optimized geometry is exactly the same when the two monomers are placed at 3 and 4 Å, and all parameters have the

same values. The geometry obtained starting with the monomers at 5 Å is not parallel anymore: the connection is formed only at one end of the monomers. (Table II.12)

**Table II.12. Relative energies, weak interactions and the graphical representations of the parallel 3<sub>10</sub>-dimer (initial structure based on canonical form)**

Initial structure based on canonical form						
						
Distance (Å)	ΔE	C=O...H(CH)	C=O...H(CH <sub>3</sub> )	Other interactions	Length (Å)	Graphical representation
2	5.86		O15-H119		2.51	
			H45-O117		2.45	
			H71-O144		2.51	
3	24.11		O24-H138		2.45	
		O51-H133			2.49	
			O51-H165		2.49	
		H58-O126			2.24	
			H63-O98		2.40	
				O78-H186(carb)	1.71	
				H80-O185(carb)	2.56	
4	24.11		O24-H138		2.45	
		O51-H133			2.49	
			O51-H165		2.49	
		H58-O126			2.24	
			H63-O98		2.40	
				O78-H186(carb)	1.71	
				H80-O185(carb)	2.56	
5	9.56	H22-O162			2.33	
			O24-H137		2.40	
			H26-O135		2.33	

## II.4.3. Conclusions

### *Perpendicular dimers*

Optimizations of  $\alpha$ ,  $\pi$ ,  $3_{10}$  helices placed at 2.5-3 Å lead to perpendicular structures independent of the starting dimers. The geometries obtained from the optimizations of nearly all  $3_{10}$  helices are perpendicular. Optimization of perpendicular  $\beta$  dimers led only once to perpendicular direction (4 Å). In turn the structure described by DeSantis does not yield perpendicular dimers after the optimizations. In the case of  $\alpha$  and DeSantis dimers the most stable structures are parallel. This is not valid for  $\pi$ ,  $3_{10}$  and  $\beta$  dimers, their most stable geometries are neither parallel nor perpendicular.

### *Antiparallel dimers*

Geometry optimization of the antiparallel placed units result in antiparallel structures. This is valid for all the five dimers. It can be clearly stated that the antiparallel structures are the most stable when the distances between the units are 2-4 Å. The intermolecular energies are around 0.7 kcal/mol if the  $3_{10}$  monomers are positioned at 1.5-3.5 Å. The other intermolecular interaction adds around 3 kcal/mol to the stabilization energy.

### *Parallel dimers*

The geometry optimizations of the previously optimized  $\alpha$  monomers led to parallel structures no matter how large the distance between the starting molecules was. Only the  $\alpha$  structures based on canonical form laid at 1-3 Å kept the parallel structures. The most stable structures are formed when the antecedently optimized monomers are laid at 3-4 Å. In this case the intermolecular energy is 3.34 kcal/mol.

The relative energy values obtained by the optimization of  $\pi$  monomers are very close. Therefore it is very difficult to determine which is the most stable geometry. The intermolecular energy depends on the starting structure. The optimized dimers of the structure based on the canonical form have more intermolecular interactions, but the intermolecular energy normalized per interaction is much smaller (~2 kcal/mol) than in the case when the starting structure is based

on the HF optimized monomer. In no case will the optimized dimers have parallel structures; the parallel-placed  $\pi$  monomers based on the canonical form become intertwined with each other.

The optimized dimers containing  $3_{10}$  monomers remain parallel if the two units are placed at 2-3 Å independently from starting structures, but they are a slightly shifted relative to each other. The most stable structure is obtained when the monomers based on canonical form are at 3 and 4 Å distance, the 'per-interaction' intermolecular energy is 3 kcal/mol.

Geometry optimizations of monomers which are further than 1 Å were not successful. If the starting structure is based on the HF optimized monomer, the obtained structure is parallel. Coiled dimers were obtained from the monomers based on the canonical form.

The most stable structure was obtained when the optimized monomers of structure described by DeSantis are located at 3 Å, but the initial orientations of the monomer were not maintained.

## II.5. Spectroscopic predictions on PLA secondary structure elements

Spectroscopic parameters were predicted for helical ( $\alpha$ ,  $\pi$ , 103) and  $\beta$ -sheet structures, in an attempt to aid our on-going efforts in the synthesis and characterization of poly(lactic acid) variants. The methods tested here include density functional (M062X/6-31G\*, M062X/6-31G\*\*, solvated M062X/6-31G\*\*) applied with standard convergence criteria as defined in Gaussian 09. Spectral parameters were invoked using the commands Freq and NMR. In terms of the importance of solvation, this is estimated by comparing values computed in water (as a limit of very polar medium) and vacuum (as a limit of completely non-polar medium).

### II.5.3. Results and Discussion

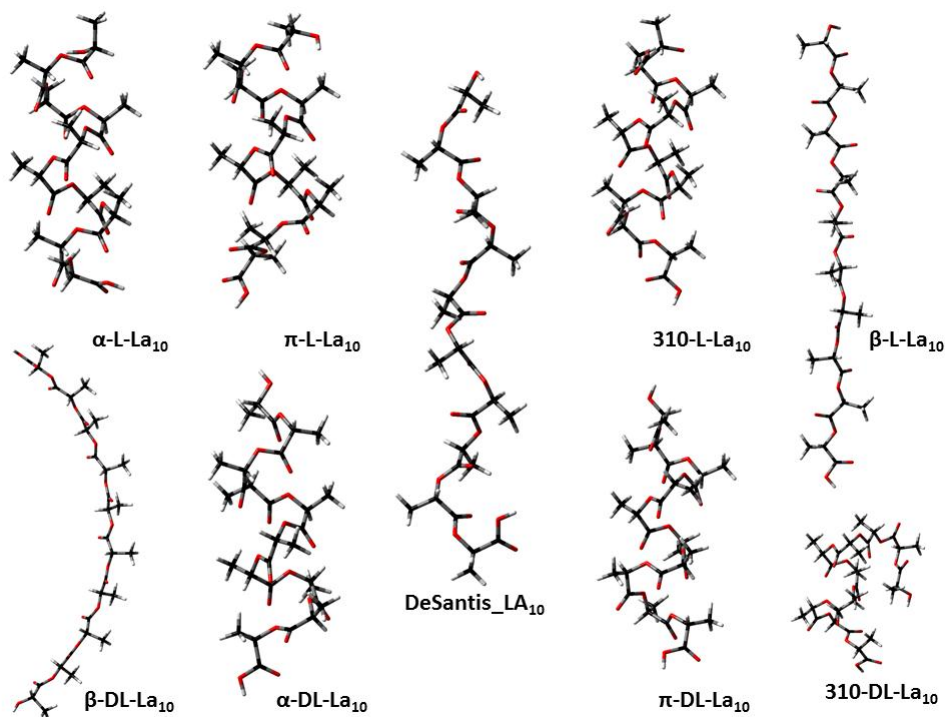
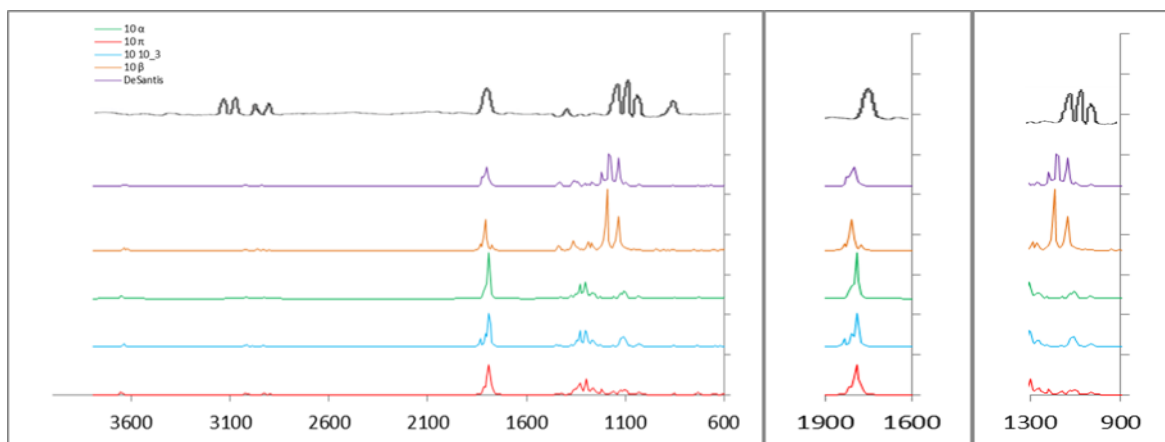


Figure II.3. Graphical representation of polylactic acid geometries optimized by DFT

### II.5.3.1. IR analysis

The vibrational frequencies were computed for these optimized structures. In addition it was calculated the vibrational frequencies of the polylactic structure described by DeSantis. Figure II.4 shows the IR spectra of the computed and prepared polylactic acids. In the experimental IR spectra can be seen the bands of C=O stretching ( $1751,20\text{ cm}^{-1}$ ), C-OC stretching ( $1117,42\text{ cm}^{-1}$ ) and CH bending and C-OC stretching ( $1064,37\text{ cm}^{-1}$ ). Thus, in general, the IR spectra shows characteristic bands mainly due to methylene and carboxylic C=O bonds. A repeat unit of PLA consists of three skeletal bonds: C-O, O-C $_{\alpha}$ , C $_{\alpha}$ -C. For PLA the bands are assigned due to backbone bond stretching (C-O, O-C $_{\alpha}$ , C-C $_{\alpha}$ ), backbone bond angle bending (O-C-C $_{\alpha}$ , C-O-C $_{\alpha}$ , O-C $_{\alpha}$ -C), for the side branches the bending (O-C $_{\alpha}$ -C $_{\beta}$ , C-C $_{\alpha}$ -C $_{\beta}$ , C $_{\alpha}$ -C=O) and stretching (C $_{\alpha}$ -C $_{\beta}$ , C=O).

The intensity of computed IR vibrations depends on the structure of the poly(lactic acid).



**Figure II.4. IR spectra of PLLA (M062x/6-31G\*\*):(a) entire spectrum; (b) carbonyl stretch region; (c) backbone stretch region**

The IR spectra of the five structures show the same number of bands. As expected, the solvation does not involve any additional band. The bands below  $225\text{ cm}^{-1}$  are mainly due to the skeletal torsion. The  $225\text{-}925\text{ cm}^{-1}$  region bands are assigned due to the bending of the side branches. These show no significant intensities. The CH $_3$  group is responsible for the appearance of the band in the  $925\text{-}1110\text{ cm}^{-1}$  region due to the rocking vibrations. The solvation increases the intensities in the case of the three helical structures.

The C-CH<sub>3</sub> and C-OC stretching cause the presence of bands in the 1124-1213 cm<sup>-1</sup> backbone stretching region. The intensities of the bands corresponding to C-CH<sub>3</sub> stretch are medium in the case of the helical structures; the water double these values. The β-sheet and the structure described by DeSantis provide weak bands. C-OC stretching bands are shown in the 1151-1217 cm<sup>-1</sup> region. In the β-sheet this band is the most intense, six times higher than the others. The solvation increases the intensity further. The structure described by DeSantis has a strong band in this region.

In the 1215-1412 cm<sup>-1</sup> region can be seen bands assigned to CH, CH<sub>3</sub> bending and C-O-C stretching. The intensity of the CH bending and C-O-C stretching in the case of β-sheet and the structure described by DeSantis are very strong in contrast with the helical structure. These are the highest intensity bands in the entire spectrum. The solvent does not influence these intensities. The CH bending intensities are roughly the same with the exception of the structure described by DeSantis. The solvation increases the intensities in the case of the helical structures. Different medium band appear in this region due to the CH bending and CH<sub>3</sub> scissoring. It is worth noting the assignments in the 1407-1437 cm<sup>-1</sup> region. In this interval appear the bands due to CH<sub>3</sub> scissoring vibrations. In the case of the three helical structures do not show significant intensities, but in the case of the β-sheet the intensity is notable.

The IR spectra of the PLLA in the range of 1865-1932 cm<sup>-1</sup> appears to be distinct for each of the five conformations. There is not much difference between the C=O stretching intensities calculated by DFT/M062x/6-31G\*\* method. In turn the solvation increases the intensities in all five structures. The five conformers exhibit single absorption bands, spaced by about 9 and 18 cm<sup>-1</sup> from each other.

The CH stretching, the symmetric and asymmetric stretching of CH<sub>3</sub> result in the appearance of weak bands in the 3050-3191 cm<sup>-1</sup> CH spectral region. It can be seen that the stretching frequencies are higher than the corresponding bending frequencies.

The calculated frequencies (cm<sup>-1</sup>) and peak band assignment for the 3<sub>10</sub> helical structures of PLLA are shown in tables II. 59.

**Table II.13. Peak band assignments for 3<sub>10</sub>-L-LA<sub>10</sub>**

3 <sub>10</sub> -L-LA <sub>10</sub>				
M062X 6-31G**		M062X 6-31G** water		Assignment
v(cm <sup>-1</sup> )	Intensity	v(cm <sup>-1</sup> )	Intensity	

19-226	0-11	17-214	0 -8	skeletal torsion
234-281	0-14	219-286	0-9	CH <sub>3</sub> rocking
299-400	0-58	295-396	0-170	CH <sub>3</sub> wagging
409	22	399	141	OH (free) bending
410-416	9-40	403-406	4-8	CH <sub>3</sub> wagging
419	4	407	5	OH (free) bending
425-588	1-230	410-596	1-135	CCO bending
636	70	644	63	OH (COOH) bending
655-788	0-35	660-775	0-50	C=O bending
824	14	842	21	C-CO (carboxyl) stretching
878-910	1-45	891-909	1-37	CH <sub>3</sub> bending + COC bending
925-1106	1-93	925-1099	0-217	CH <sub>3</sub> rocking
1127-1164	15-106	1104-1161	41-232	C-CH <sub>3</sub> stretching
1167-1189	5-146	1162-1185	3-213	C-OC stretching
1222-1331	3-89	1213-1329	8-369	CH bending + C-OC stretching
1332-1372	11-403	1331-1365	4-938	CH bending
1373-1403	6-182	1367-1402	11-311	CH bending + CH <sub>3</sub> scissoring
1412-1426	3-88	1407-1421	12-80	CH <sub>3</sub> scissoring
1445	28	1430	1430	CH <sub>3</sub> twisting (COOH end)
1448	83	1445	120	CH <sub>3</sub> twisting (OH end)
1495-1528	0-46	1486-1518	1-33	CH <sub>3</sub> twisting
1875-1931	32-756	1852-1894	57-1074	C=O stretching
3078-3094	7-10	3071-3091	9-17	CH <sub>3</sub> sym stretching
3115-3152	1-9	3120-3154	4-13	CH stretching
3171-3193	0-14	3159-3194	2 -25	CH <sub>3</sub> asym stretching
3826	62	3850	75	OH (free) stretching
3830	100	3807	159	OH (COOH) stretching

Comparing the calculated data with the experimental data it can be seen that the calculated frequency values are bigger than the experimental values.

### II.5.3.2. NMR

The shifts within the <sup>13</sup>C NMR spectrum of the four secondary-type structure of PLLA calculated by DFT/M062x/6-31G\*\* method are larger than those calculated in solvated models

(Table II.14). The  $^1\text{H}$  NMR chemical shifts of PLLA are not always smaller in solution (Table II.15). Taking into account all five NMR signals covered by these two tables, the  $\beta$  and  $\pi$  structures appear to generally yield the closest values to the experiment.

**Table II.14. Computed and experimental  $^{13}\text{C}$  NMR Chemical shifts ( $\delta$ , in ppm) of CO, CH and  $\text{CH}_3$  of PLLA**

PLLA	$\alpha$		$\pi$		$10_3$		$\beta$		Experimental data
	vacuum	water	vacuum	water	vacuum	water	vacuum	water	
$\delta$ (CO)	177,61	174,97	178,15	175,25	177,10	174,96	175,31	172,34	171,72
$\delta$ (CH)	71,88	68,05	72,14	68,12	71,83	67,98	71,68	67,12	65,88
$\delta$ ( $\text{CH}_3$ )	18,51	12,91	18,69	13,14	18,27	13,29	18,98	13,51	16,71

**Table II.15. Computed and experimental  $^1\text{H}$  NMR Chemical shifts ( $\delta$ , in ppm) of CH and  $\text{CH}_3$  of PLLA**

PLLA	$\alpha$		$\pi$		$10_3$		$\beta$		Experimental data
	vacuum	water	vacuum	water	vacuum	water	vacuum	water	
$\delta$ (CH)	5,15	5,10	5,07	5,07	5,17	5,07	5,30	5,47	4,93
$\delta$ ( $\text{CH}_3$ )	1,67	1,71	1,66	1,63	1,68	1,67	1,65	1,62	1,45

## II.5.4. Conclusions

The calculated chemical shifts of both  $^{13}\text{C}$  NMR and  $^1\text{H}$  NMR are slightly larger than the experimental one. The solvation reduces the value of the NMR chemical shifts.

## II.6. Polylactic acid interactions with bioceramics surfaces

Molecular dynamics simulations were employed to study polylactic acid/bioceramics interface interactions. The study analyzed the binding energies between polylactic acid and two bioceramics: hydroxyapatite and zirconia. The interactions of polylactic acid on the surfaces

crystallographic planes (0 0 1), (1 0 0), (1 1 0), (1 1 1) and (-1 0 0) were simulated. The effects of coupling agents on interfacial binding energies were also examined.

### II.6.3. Results and discussions

The adhesion between the polylactic acid and bioceramic surfaces can be evaluated by the interaction energy between them. The interaction energies were calculated through the following equation:

$$E_{\text{interaction}} = E_{\text{surface+polymer}} - (E_{\text{surface}} + E_{\text{polymer}}) \quad (1)$$

where  $E_{\text{surface+polymer}}$  is the energy of the surface with PLA polymer,  $E_{\text{surface}}$  is the energy of the surface and  $E_{\text{polymer}}$  is the energy of the polymer. The binding energy is obtained by dividing the interaction energy to the number of monomers existing in the polymers. The high binding energy suggests high adhesive strength between the surface and the polymer.

The coupling agents increase molecular binding between bioceramics and polymers. The interaction energies in surface/coupling agent/polymer system

$$E_{\text{interaction}} = E_{\text{surface+coupling agent+polymer}} - (E_{\text{surface+coupling agent}} + E_{\text{polymer}}) \quad (3)$$

where  $E_{\text{surface+coupling agent+polymer}}$  is the energy of the surface with silane and PLA polymer,  $E_{\text{surface+coupling agent}}$  is the energy of the surface with silane and  $E_{\text{polymer}}$  is the energy of the polymer. The interaction energies of polylactic acid/zirconia and polylactic acid/silane/zirconia systems are listed in **Error! Reference source not found.** The negative number indicates that the polymer is binding to the surface. It can be observed that in all cases the different types of polylactic acids are binding to the zirconia surface

Molecular dynamics simulations were employed to study polylactic acids/ hydroxyapatite interfaces interactions. Table II.16 **Error! Reference source not found.** shows the interaction energies of different optimized polylactic acids and hydroxyapatite systems with and without coupling agents. The polylactic acids bind to the polymers. There is one exception, optimized  $\alpha$  helix did not attached to the (1 1 1) hydroxyapatite surface. It can not clearly establish which structure has the biggest adhesion to all hydroxyapatite surfaces. The optimized  $\pi$  and  $\beta$  decameric units are hardly linked to (0 0 1) and (1 1 0) surfaces, respectively. The optimized structure described by DeSantis bind to (0 0 1), (1 1 0), (1 1 1) and (-1 0 0) hydroxyapatites with

interaction energies above 4 kcal/mol. 3-6 kcal/mol interaction energies exist between optimized  $\pi$  helices and (1 1 0), (1 1 1) and (-1 0 0) surfaces. The interface energies are around 4-5 kcal/mol when the  $3_{10}$  structures are connected to (1 1 0) and (-1 0 0) hydroxyapatite surfaces.

**Table II.16. The interaction energies of polylactic/hydroxyapatite and polylactic acid/silane/hydroxyapatite systems**

h k l	PLA	$E_{\text{interaction}}$ (kcal/mol)	
		PLA/zirconia	PLA/silane/zirconia
(0 0 1)	$\alpha$ -L-LA <sub>10</sub>	-0.79	-17.46
	$\pi$ -L-LA <sub>10</sub>	-0.07	-11.44
	$3_{10}$ -L-LA <sub>10</sub>	-1.52	-22.67
	$\beta$ -L-LA <sub>10</sub>	-1.95	-15.77
	DeSantis-LA <sub>10</sub>	-3.90	-31.63
(1 0 0)	$\alpha$ -L-LA <sub>10</sub>	-1.50	-11.78
	$\pi$ -L-LA <sub>10</sub>	-1.13	-18.54
	$3_{10}$ -L-LA <sub>10</sub>	-2.16	-10.57
	$\beta$ -L-LA <sub>10</sub>	-2.60	-29.59
	DeSantis-LA <sub>10</sub>	-0.47	-12.48
(1 1 0)	$\alpha$ -L-LA <sub>10</sub>	-0.84	-9.64
	$\pi$ -L-LA <sub>10</sub>	-4.76	-12.05
	$3_{10}$ -L-LA <sub>10</sub>	-4.96	-0.36
	$\beta$ -L-LA <sub>10</sub>	-0.18	-8.32
	DeSantis-LA <sub>10</sub>	-6.63	-12.74
(1 1 1)	$\alpha$ -L-LA <sub>10</sub>	0.46	-12.33
	$\pi$ -L-LA <sub>10</sub>	-3.13	-8.60
	$3_{10}$ -L-LA <sub>10</sub>	-1.24	-7.80
	$\beta$ -L-LA <sub>10</sub>	-2.74	-17.27
	DeSantis-LA <sub>10</sub>	-6.16	-9.20
(-1 0 0)	$\alpha$ -L-LA <sub>10</sub>	-1.84	-15.68
	$\pi$ -L-LA <sub>10</sub>	-5.98	-4.30
	$3_{10}$ -L-LA <sub>10</sub>	-3.99	-15.90
	$\beta$ -L-LA <sub>10</sub>	-3.68	-27.32
	DeSantis-LA <sub>10</sub>	-5.41	-15.26

Silanes have a much greater effect on the polymer/hydroxyapatite interactions than in the case of polylactic acid/zirconia systems. The adhesion of optimized  $\pi$  helix increases 155 times with the addition of coupling agent (Figure II.5). However the interaction energy decrease when the helix is attached to (-1 0 0) hydroxyapatite in the presence of silane.

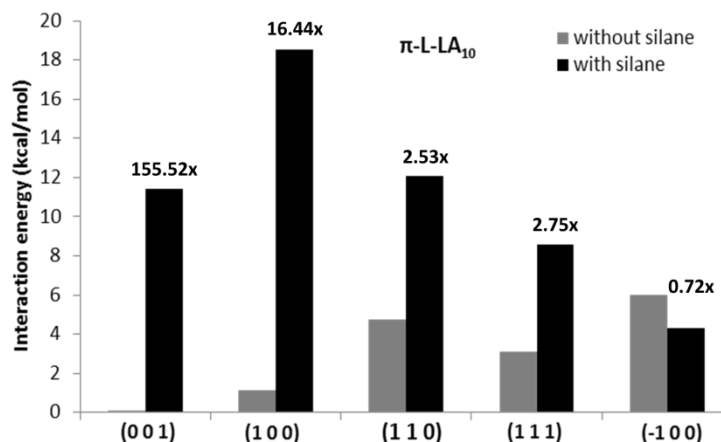


**Figure II.5. The interaction energy of the optimized  $\pi$  helices/hydroxyapatite surfaces without and with coupling agents**

The general formula of hydroxyapatite is  $\text{Ca}_{10}(\text{PO}_4)_6(\text{OH})_2$ . The top layers of the surfaces have different atom compositions by cleaving the crystal along planes. Oxygen, calcium and phosphorus atoms are at the (1 0 0), (1 1 0) and (-1 0 0) surfaces. The interface of (0 0 1) hydroxyapatite contains oxygen and hydrogen molecules. Oxygen, hydrogen and phosphorus atoms constitute the top layers of (1 1 1) surface. Weak interactions hold together polylactic acids and hydroxyapatite systems. These interactions are formed between the hydrogen atoms from methyl groups or from the main chains of the polylactic acids and the oxygens of the surfaces. Attractions exist between oxygen from ester groups of polylactic acids and hydroxyl groups in hydroxyapatite. Polylactic acids change their conformations after molecular dynamic simulations due to the interactions. The polymers did not remain parallel with the surface (Figure II.6). Interactions between the polylactic acids and silane molecules exist when coupling agents are added to the system. The conformations of the decameric units were not preserved in these cases neither (Figure II.7).

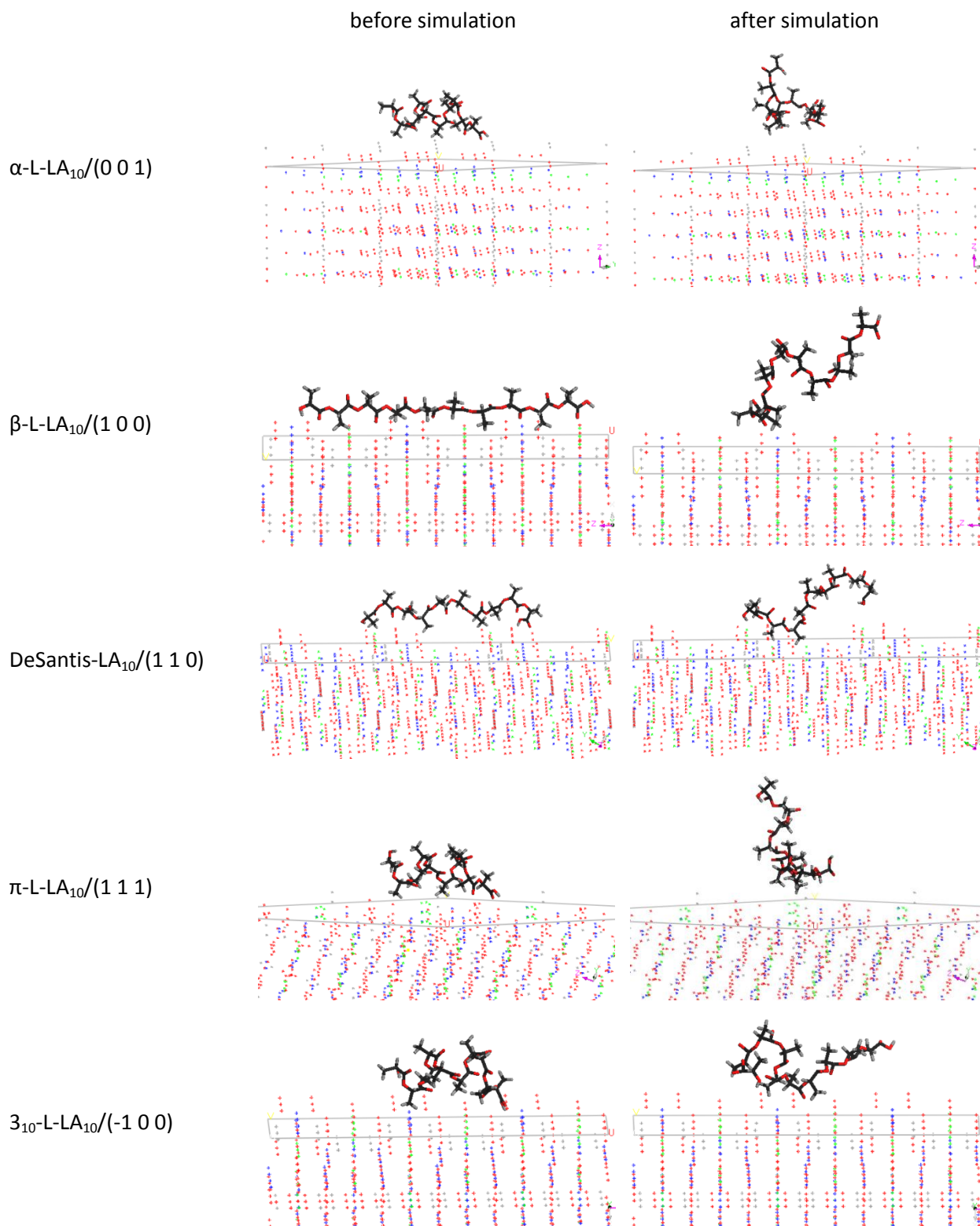


**Figure II.6. Snapshots of polylactic acids on hydroxyapatite surfaces before and after the simulations**

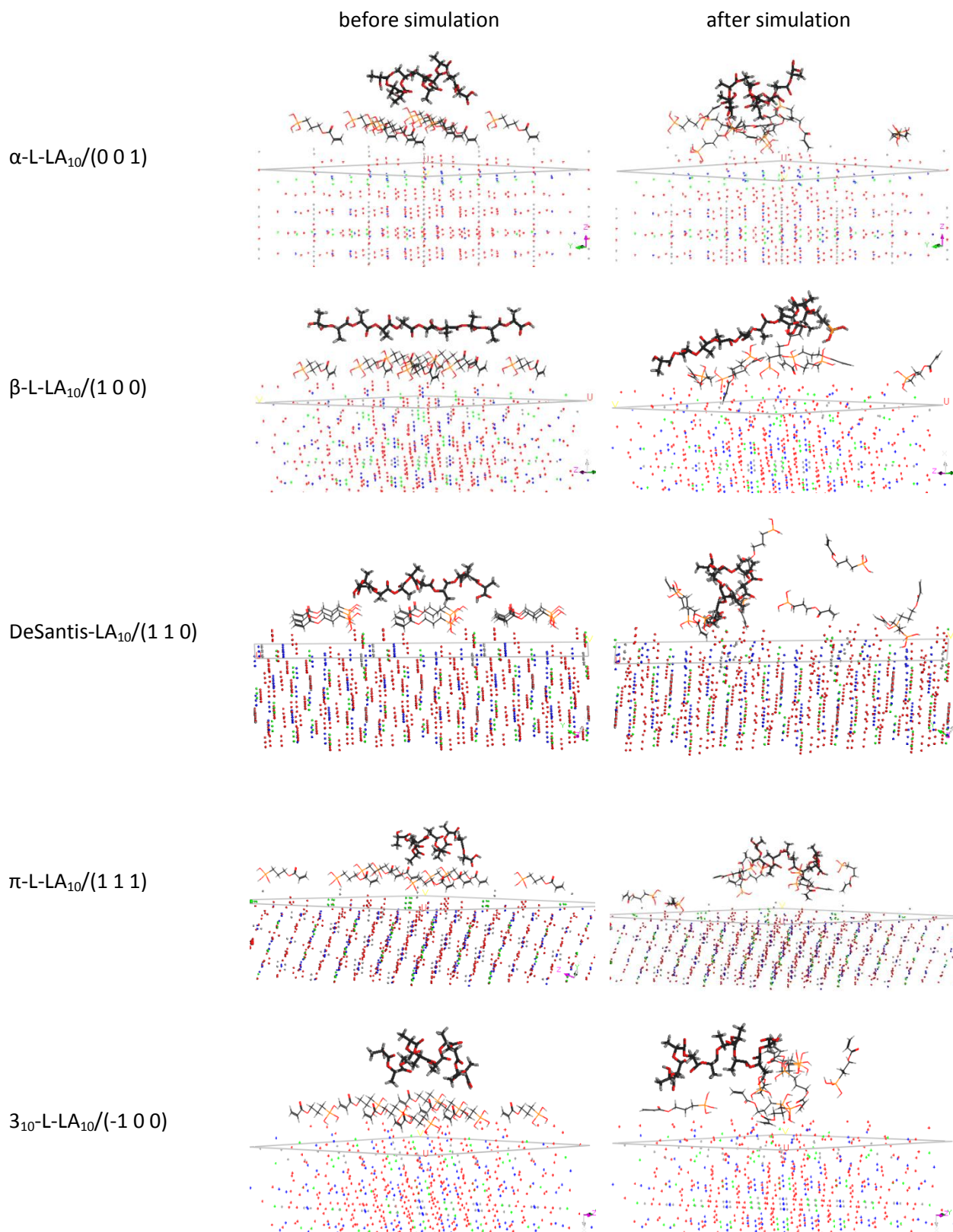


**Figure II.7. Snapshots of polylactic acids on silane/hydroxyapatite surfaces before and after the simulations**

## II.6.4. Conclusions

Molecular dynamics simulations were used to analyze the interfacial behaviors of polylactic acids and zirconia, hydroxyapatite surfaces. The interactions of polymers on five crystallographic planes were simulated. The interaction energies between the DFT optimized polymers and bioceramic surfaces was analyzed. The polylactic acids bind to the polymers in every situation. There is one exception, optimized  $\alpha$  helix did not attached to the (1 1 1) hydroxyapatite surface. Optimized  $\beta$  sheets bind most strongly to the five zirconia surfaces, the interaction energies are above 20 kcal/mol. The energy values are much smaller in polylactic acid/hydroxyapatite systems than in the polylactic acid/zirconia systems. The silane coupling agents can improve the interactions between the bioceramic surfaces and the polylactic acids. The effects of the coupling agents are more evident if the surface is hydroxyapatite.

Weak interactions hold together the polylactic acids and bioceramic systems. These interactions are formed between the hydrogen atoms from methyl groups or from the main chains of the polylactic acids and the oxygens of the surfaces. Polylactic acids change their conformations after molecular dynamics simulations due to the interactions. The conformation changes are more obvious when silane coupling agents are added to the polylactic acids and bioceramic systems.

**Chapter III**  
**Study of polyethers by mass spectrometry**

## III.2 In-source collision induced dissociation study of polyethers cationized by alkali metal ions

In-source collision induced dissociation (ISCID) of polyethylene glycol (PEG) and polypropylene glycol (PPG) cationized by alkali metal ions was studied as a function of the chain length and collision energy using electrospray ionization mass spectrometry (ESI MS). The dissociation of the sodiated, potassiated and cesiated PEG and PPG yielded a neutral polyether and a cation without the formation of product ions resulting from the backbone cleavages. The survival yield (SY) method was applied to characterize the in-source fragmentation behavior of the cationized polyethers. The SY curves obtained by tandem MS/MS CID and in-source CID were compared. A remarkable difference was found, i.e. increasing the collision energy, the polyethers entirely dissociate in the collision cell, while the in-source SY plots level off at about 0.1-0.3. The finite SY values at large ISCID collision energies may suggest ion-molecule reactions in the ISCID region of the instrument. It was found that the characteristic ISCID<sub>50</sub> collision energy corresponding to SY=0.5 was dependent linearly on the number of the repeat units, i.e., on the size of the polyethers.

### III. 2.1 Experimental section

#### III.2.1.3. Determination of the ISCID<sub>50</sub> values

$$SY = (1 - \alpha) \frac{1}{1 + ae^{b_{CE}}} + \alpha \quad (4)$$

The ISCID<sub>50</sub> values can be obtained by fitting the parameters of the three-parameter modeling function (Eq. (4)) to the experimental data utilizing a spreadsheet software and expressing the value of the in-source collision energy at SY=0.5 (ISCID<sub>50</sub>).

### III.2.2 Results and Discussion

In order to study the in-source collision induced dissociation of sodiated and potassiated polyethers the solutions of polyethylene glycol, NaCl and KCl, and polypropylene glycol, NaCl and KCl were directly injected into the ESI source at varying ISCID voltage. The dissociation of PEG and PPG yielded a neutral polyether and a cation without the formation of product ions resulting from the backbone cleavages. Only the decrease of the precursor ion signal intensity with increasing in-source collision voltage could be observed, whereas the parallel increase of the cation signal could not be detected since the low masses of these cations fell below the lowest mass limit on our mass analyzer. In order to get proof for this fragmentation channel CsCl was used as an ionization agent. By the increase of the ISCID energy, the decrease of the cesiated PEG and PPG intensity with the parallel increase of the Cs<sup>+</sup> ion signal intensity was observed, which proves that the dissociation of the cationized PEG and PPG yielded a neutral polyether and a cation. As a representative example, Figure III.1 shows the ESI-MS spectrum of PEG recorded at 70 eV ISCID energy. As seen in figure, the intensity of the lower molecular weight potassiated PEGs is suppressed, which reflects the molecular weight dependence of the cation dissociation and the difference between the sodium and potassium dissociation energy, as it will be discussed later.

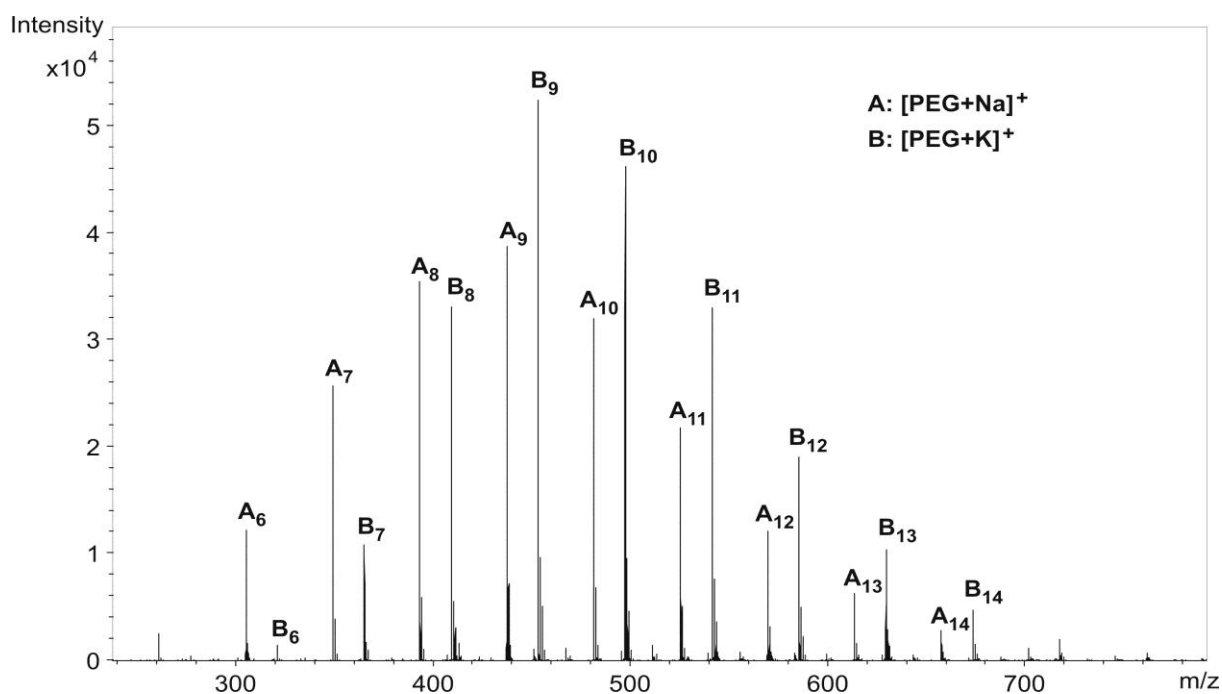


**Figure III.1. ESI-MS spectrum of PEG recorded at 70 eV ISCID energy. The ratio of the ionization agents is Na+:K+ 4:1 (v/v). The numbers in the subscripts represent the numbers of the PEG monomeric units.**

The survival yield (SY) method was used for the evaluation of the energy dependence of the dissociation processes of cationized polyethers into neutral polyether and the cation.

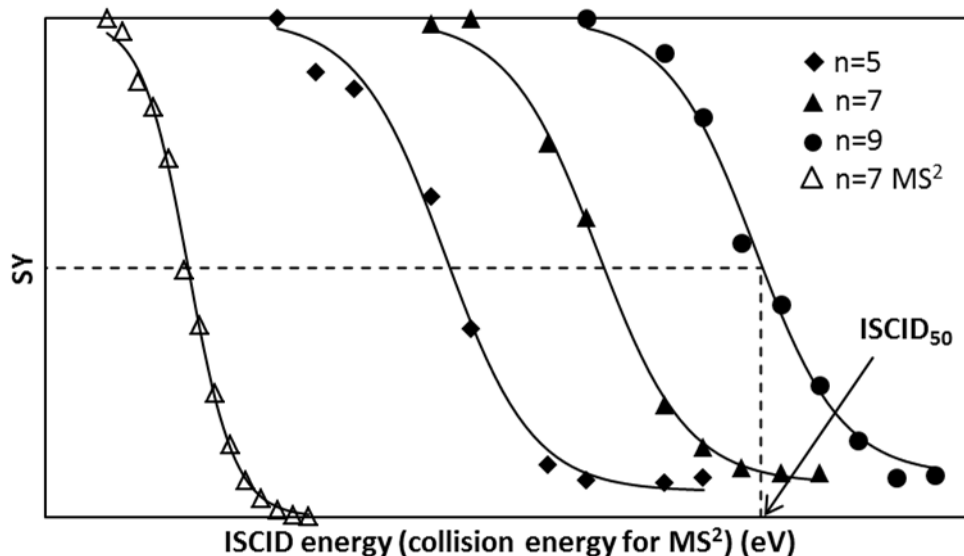


**Figure III.2. Survival yield (SY) versus ISCID energy curve for the potassiated PPG5, PPG7 and PPG9 (PPG with 5, 7 and 9 monomeric units, respectively). The empty triangles represent the MS/MS SY curve recorded by QqTOF of the potassiated PPG7. The solid lines represent the fitted curves by Eq. (4). The fitted parameters are:  $a=1.814 \times 10^{-5}$ ,  $b=0.1771$  and  $\alpha=0.0519$  for PPG5,  $a=7.768 \times 10^{-7}$ ,  $b=0.1730$  and  $\alpha=0.0678$  for PPG7,  $a=1.537 \times 10^{-8}$ ,  $b=0.1773$  and  $\alpha=0.0840$  for PPG9, and  $a=7.179 \times 10^{-5}$ ,  $b=0.3351$  and  $\alpha=0$  for PPG7 recorded by QqTOF MS/MS.**

As seen in figure III.3, the SY curves are shifted to higher ISCID energy when the number of monomeric units is increased. This shift can be expressed with the characteristic ISCID<sub>50</sub> energy corresponding to SY=0.5, where the intensity of the examined polyether decreases to the half. For comparison the MS/MS SY curve of the potassiated PPG7 is also presented in Figure III.2. The large gap between the PPG7 plots may be due to the different conditions of the collision induced dissociation experiments in the source region and in the quadrupole collision cell of our ESI QqTOF instrument (e.g. different time scale and pressure). The comparison shows another remarkable difference: by increasing the collision energy, PPG entirely dissociates in the collision cell, while the ISCID SY plots level off at about 0.1. These

finite SY values at large ISCID collision energies can be observed for all the other polyether samples, and can be presented very expressive by plotting the intensity ratio of sodiated and potassiated peaks ( $I_{Na}/I_K$ ) versus ISCID collision energy, as shown in Figure III.3 for PEG8.

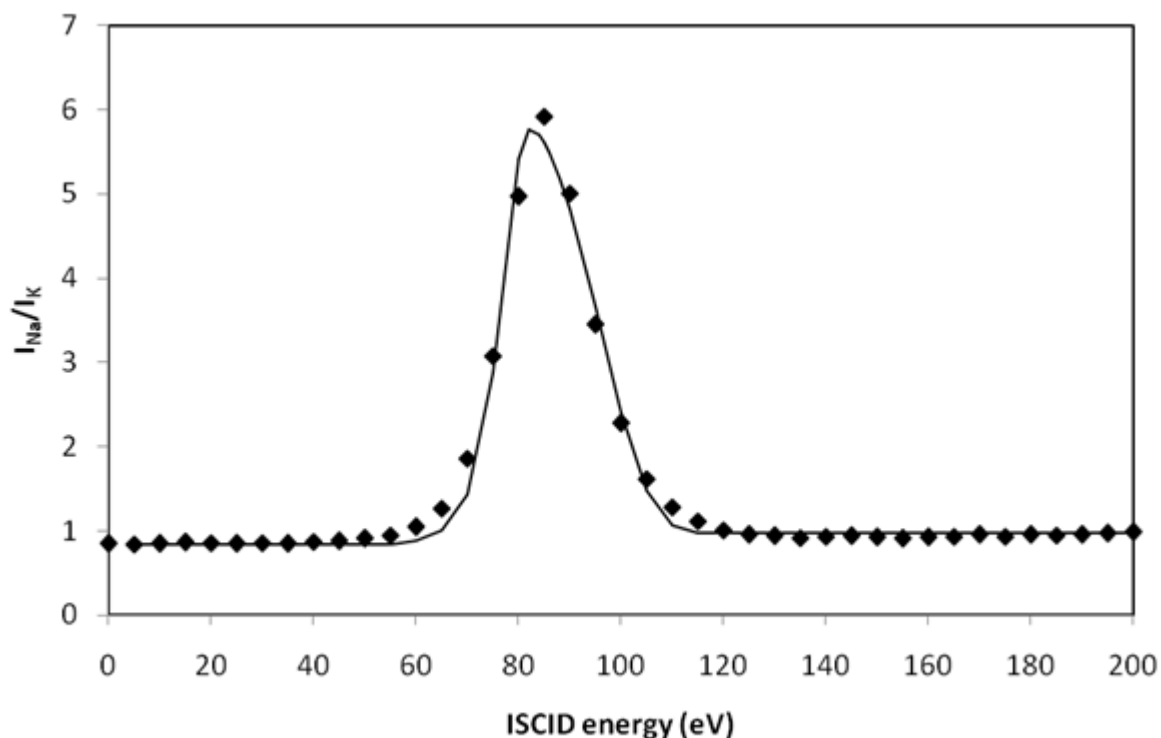


**Figure III.3. Intensity ratio of sodiated and potassiated peaks ( $I_{Na}/I_K$ ) versus ISCID energy for PEG8 (PEG with 8 monomeric units). The solid lines represent the fitted curve applying Eq. (4) for fitting  $I_{Na}$  and  $I_K$ .**

A curve with a maximum is generated for both polyethers at various chain lengths – like the example in figure III.4 – instead of a monotonically increasing curve, which one can expect on the basis of the energy dependent MS/MS experiments for the  $I_{Na}/I_K$  versus excitation energy function. A possible explanation for the finite SY values at large ISCID collision energies (can be seen in Fig. 3) and for the  $I_{Na}/I_K$  plots (in Figure III.3) may be that ion-molecule reactions can occur in the ISCID region. The sodiated and potassiated polyether ions may collide with neutral polyethers, which already have lost their cation, and charge transfer may take place. The value of

the final leveling SY value was observed to be influenced by the cationization agent added to the polyether solution.

In order to demonstrate the effect of the size on the in source CID of polyethers, the  $ISCID_{50}$  values plotted as a function of  $m/z$  for the sodiated, potassiated and cesiated PEG and PPG are shown in Figures III.6a and Fig III.6b, respectively. The  $ISCID$  collision energy values belonging to the maximum of the  $I_{Na}/I_K$  plots (Figure III.3) versus  $m/z$  functions for PEG and PPG are presented in Figure III.6c. This latter representation of the size effect eliminates the mass discrimination of the instrument, because the characteristic energy (which is plotted as the function of the chain length) is determined on the basis of intensity ratios of close mass peaks not on the basis of intensities.

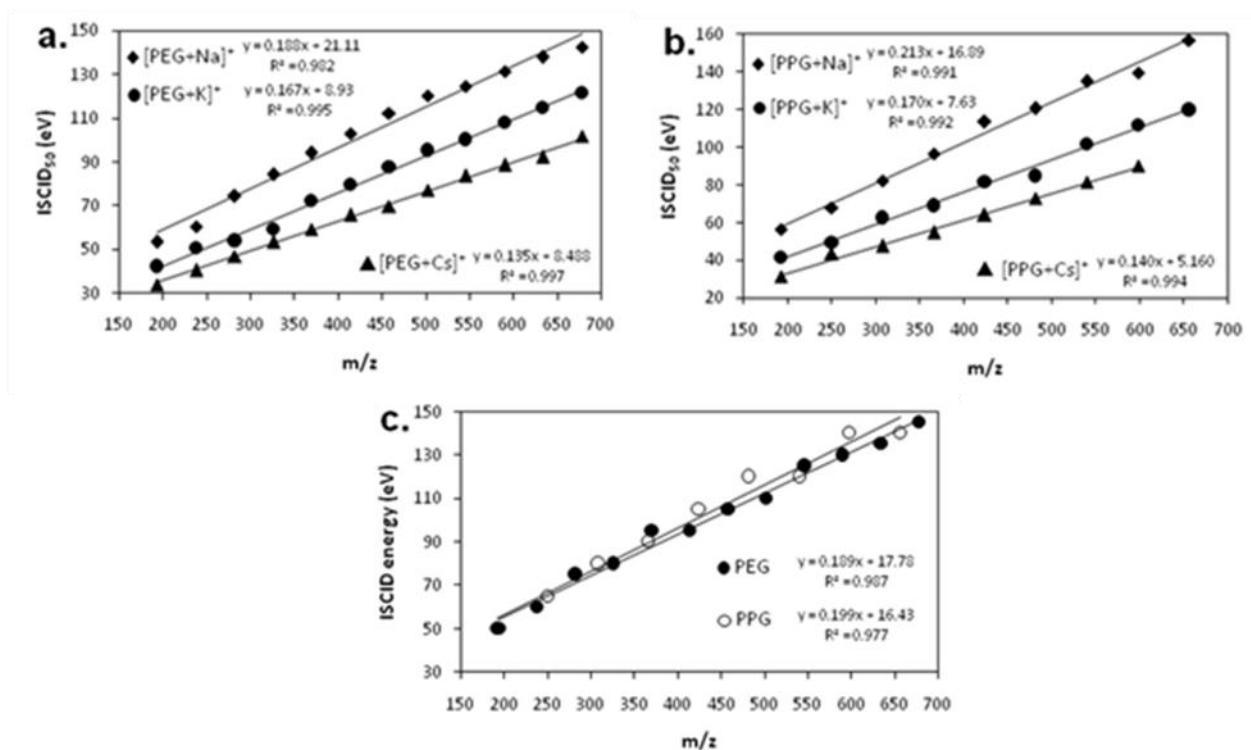


**Figure III.4.** The variation of  $ISCID_{50}$  value with  $m/z$  for the sodiated, potassiated and cesiated PEG (a) and PPG (b). The variation of  $ISCID$  energies – belonging to the maximum point of the  $I_{Na}/I_K$  versus  $ISCID$  energy plots – with  $m/z$  for PEG and PPG (c).

As seen in figure III.6 a,b, the  $ISCID_{50}$  values vary linearly with the size of the polyethers. Also a good linearity can be observed, if the  $ISCID$  energies at the maximum point of the  $I_{Na}/I_K$

versus ISCID energy plots are plotted as a function of the  $m/z$  of the polyethers, confirming the linear correlation between the  $ISCID_{50}$  – polymer size values.

In order to establish the possible concentration and ion ratio dependence of the  $ISCID_{50}$  values and the ISCID collision energy values belonging to the maximum of the  $I_{Na}/I_K$  plots, experiments were performed at different polyether concentrations and at different ionization agents (NaCl, KCl, LiCl) and ionization agents ratios as detailed in the Experimental section. It was found, that neither the  $ISCID_{50}$  values nor the  $I_{Na}/I_K$  plot maximum points depend on the polyether concentrations and on the ionization agents.

### **III.2.3 Conclusions**

The presented results show remarkable differences between QqTOF tandem mass spectrometric CID and the ESI in-source CID for the single sodiated and potassiated PEG and PPG dissociation into neutral and a cation. The characteristic energies corresponding to 50% fragmentation are notably higher at ISCID. Moreover, the dissociation of the PEG and PPG resulted zero survival yields at high collision energies by QqTOF CID, while fragmenting the polyethers by ISCID finite leveling SY values at about 0.1-0.3 were observed presumably due to ion-molecule reactions in the ISCID region.

A linear relationship was found between the characteristic energy of ISCID fragmentation and the mass of polyethers.

## General conclusions

This study presents the synthesis, molecular modeling of polylactic acid and characterization of polypropylene glycol and polyethylene glycol.

Enzymatic polymerizations of lactic acid have been investigated. The influences of parameters were examined to determine the optimum conditions of synthesis. The best results were obtained by the polymerization of DL-lactic acid at 40 °C, in the presence of hexane solvent and at 24 h reaction time.

Theoretical studies have been carried out on four secondary-type structures ( $\alpha$ ,  $\pi$  and  $10_3$  helical structures and  $\beta$ -sheet) and on structure proposed by DeSantis of polylactic acid to search the possible secondary structure-like motifs. Computational predictions on the relative stabilities and structural details differ significantly between empirical, semiempirical and ab initio methods. Three types of weak interactions appear to dictate the relative stabilities of secondary structure elements in polylactic acid structures. These non-covalent interactions involve the oxygen atom of the carbonyl group and atoms of neighboring monomers in the primary structure, as follows: (1) the hydrogen atom of the CH group in lactic acid, (2) a hydrogen atom in the methyl group, and (3) the oxygen atom of an ester group. Computational predictions anticipate the presence of another distinct structural motif called turns based on a Ramachandran-like analysis.

Inter-strand supramolecular interactions between PLA units were examined as part of an effort ultimately aiming to provide useful data for predicting and controlling macroscopic properties of PLA-based materials. Parallel, antiparallel as well perpendicular dimers were considered.

A vibrational analysis and NMR simulation has been carried out to analyze the secondary structure of poly(lactic acid) resulted from esterification of ten lactic acid units.

Molecular dynamics simulations were used to analyze the interfacial behaviors of polylactic acids and zirconia, hydroxyapatite surfaces. The interactions of polymers on five crystallographic planes were simulated. The silane coupling agents can improve the interactions between the bioceramic surfaces and the polylactic acids. The effects of the coupling agents are more evident if the surface is hydroxyapatite. Weak interactions hold together the polylactic acids

and bioceramic systems. These interactions are formed between the hydrogen atoms from methyl groups or from the main chains of the polylactic acids and the oxygens of the surfaces. Polylactic acids change their conformations after molecular dynamics simulations due to the interactions. The conformation changes are more obvious when silane coupling agents are added to the polylactic acids and bioceramic systems.

In-source collision induced dissociation (ISCID) of polyethylene glycol (PEG) and polypropylene glycol (PPG) cationized by alkali metal ions was studied as a function of the chain length and collision energy using electrospray ionization mass spectrometry (ESI MS). The presented results show remarkable differences between QqTOF tandem mass spectrometric CID and the ESI in-source CID for the single sodiated and potassiated PEG and PPG dissociation into neutral and a cation. The characteristic energies corresponding to 50% fragmentation are notably higher at ISCID. Moreover, the dissociation of the PEG and PPG resulted zero survival yields at high collision energies by QqTOF CID, while fragmenting the polyethers by ISCID finite leveling SY values at about 0.1-0.3 were observed presumably due to ion-molecule reactions in the ISCID region. The characteristic energies corresponding to 50% fragmentation are notably higher at ISCID. Moreover, the dissociation of the PEG and PPG resulted zero survival yields at high collision energies by QqTOF CID, while fragmenting the polyethers by ISCID finite leveling SY values at about 0.1-0.3 were observed presumably due to ion-molecule reactions in the ISCID region.

## **Acknowledgements**

The financial support provided from the following sources is gratefully acknowledged:  
Investing in people! Ph.D. scholarship, Project co-financed by the SECTORAL OPERATIONAL PROGRAM FOR HUMAN RESOURCES DEVELOPMENT 2007 – 2013 Priority Axis 1. "Education and training in support for growth and development of a knowledge based society"  
Key area of intervention 1.5: Doctoral and post-doctoral programs in support of research.  
Contract nr.: POSDRU/88/1.5/S/60185 – "INNOVATIVE DOCTORAL STUDIES IN A KNOWLEDGE BASED SOCIETY" Babeş-Bolyai University, Cluj-Napoca, Romania

## List of publications

### Scientific papers

1. **Secondary structure elements in polylactic acid models**, I. Irsai, C. Majdik, A. Lupan, R. Silaghi-Dumitrescu, *Journal of Mathematical Chemistry*, 2012, 50:703-733, DOI: 10.1007/s10910-011-9919-z

2. **In-source collision dissociation study of polyethers cationized by alkali metal ions**, Á. Kuki, I. Irsai, L. Nagy, G. Shemirami, C. Majdik, M. Zsuga, S. Kéki, *International Journal of Mass Spectrometry*, In press, DOI: 10.1016/j.ijms.2012.10.004

### Poster Communications

1. **Computational investigation of putative secondary structure elements in polylactic acid, and of spectroscopic parameters thereof**, I. Irsai, A. Zs. Kun, C. Majdik, R. Silaghi-Dumitrescu, *Advanced Spectroscopies on Biomedical and Nanostructured Systems*, 4-7 september 2011, Cluj Napoca, Romania

2. **Computational Investigation of Secondary Structure Elements in Polylactic Acid Models**, I. Irsai, C. Majdik, A. Lupan, R. Silaghi-Dumitrescu, XVII. Nemzetközi Vegyeszkonferencia, 3-6 noiembrie 2011, Cluj Napoca, Romania

### Oral Communications

1. **Secondary and quaternary structure in polylactic acid**, I. Irsai, A. Lupan, C. Majdik, R. Silaghi-Dumitrescu, *Molecular Modeling in Chemistry and Biochemistry*, 5-10 decembrie 2011, Cluj Napoca, Romania